

# Tuning the non-linear optical absorption properties of Eu<sup>3+</sup> doped NiWO<sub>4</sub> nanostructures

P. C. Karthika, R. A. Sharath<sup>a</sup>, K. Mani Rahulan<sup>a\*</sup>, G. Vinitha<sup>b</sup>, M. Sasidharan<sup>c\*</sup>, D.Prakashbabu<sup>d</sup>

<sup>a</sup>*Nanophotonics Research Laboratory, Department of Physics and Nanotechnology, SRM Institute of Science & Technology, Chennai-603203, India*

<sup>b</sup>*Department of Physics, School of Advanced science, Vellore Institute of Technology, Chennai-600048, India*

<sup>c</sup>*Research Institute, SRM Institute of Science & Technology, Chennai-603203, India*

<sup>d</sup>*School of Applied Sciences, REVA University, Bangalore, Karnataka, 560 064, India*

## Abstract

NiWO<sub>4</sub> nanostructures doped with different ratios of Eu<sup>3+</sup> have been prepared by a chemical precipitation method. The influence of Eu<sup>3+</sup> on NiWO<sub>4</sub> nanostructures were characterized using X-ray diffraction (XRD), UV-visible diffuse reflectance spectra, scanning electron microscopy (SEM) and Raman. XRD patterns display that the samples crystallize to monoclinic wolframite structure. SEM images reveal that the particles are well uniformly dispersed with average particle size lies around 40-50nm. Third-order nonlinear optical properties were studied by a Z-scan technique at 532 nm using continuous wave diode pumped Nd:YAG laser. Open and closed aperture results reveal the nanostructures to possess reverse saturation absorption and negative nonlinear refraction. The calculated absorption coefficients ( $\beta$ ), imaginary part of third-order susceptibilities  $\text{Im}\chi^{(3)}$  are in the order of  $10^{-6}$ (cm/W) and  $10^{-7}$  esu. These results indicated that the synthesized nanostructures could be promising materials for optical device applications.

Keywords: europium, optical properties, reverse saturable absorption, Z-scan

Corresponding author:

K. Mani Rahulan ([krahul.au@gmail.com](mailto:krahul.au@gmail.com)),  
M. Sasidharan ([sasidham@srmist.edu.in](mailto:sasidham@srmist.edu.in))

## 1. Introduction

The third order nonlinear optical (NLO) properties of nanostructured materials have become a frontier area for researchers to fabricate devices for various optical applications in areas such as photonics, telecommunications, optical switching, sensors, optical limiting etc.[1,2]. Although there are many competing materials qualifying for NLO device applications but researchers are still finding for the easy synthesizable materials with enhanced optical nonlinearity. In this regard, metal tungstates with formula  $MWO_4$  are most interesting and important inorganic materials have received attention due to their attractive size and structure dependent optical and electronic properties [3]. Such materials have found applications in scintillation counters, optical fibers and lasers [4]. Nickel tungstate ( $NiWO_4$ ) is one of the bivalent transition metal tungstate having quite interesting properties serve as an excellent candidate for applications in microwave devices [5], photocatalyst [6], etc. It is quite interesting that  $NiWO_4$  will exist in tetragonal scheelite structure when the cationic ionic radius exceed 0.099nm and exhibit monoclinic wolframite structure when the ionic radius becomes smaller than 0.077nm [7]. It is reported that crystals containing  $W^{6+}$  and cations with non-bonded electron pairs have shown to possess second order NLO behavior [8,9]. NLO studies  $PbWO_4$  with scheelite structure and  $ZnWO_4$  with a wolframite structure have reported to exhibit two photon interband absorption and two photon induced one photon absorption [10]. It is well known that the optical properties of the host are dependent on the particle size and this can be tuned by anchoring with a suitable dopant. Rare earth based materials have gained significant attention on account of their excellent optical properties inherited from intra 4f transitions [11]. Europium as rare earth cations has several advantages due to its non-degenerate ground, emitting states and  $^5D_0-^7F_0$  transition could be used as applications in luminescent devices [12]. Europium doped metal tungstates will exhibit a strong absorption at UV region as well as near blue region due to f-f transition of  $Eu^{3+}$  ions. It is reported that tungstates can effectively transfer energy to trivalent rare earth ions like europium [13]. Doping of such materials is expected to dramatically increase the optical nonlinearity of the host. Numerous methods have been employed such as co-precipitation [14], solvothermal [15], modified citrate complex technique [16], microwave irradiation [17], hydrothermal [18] for the synthesis of  $NiWO_4$  nanostructures.

In the present work we explore the third order nonlinear optical properties of Eu doped NiWO<sub>4</sub> nanostructures synthesized by chemical precipitation method. Both open and closed aperture measurements were carried out using a continuous wave Nd:YAG laser at 532 nm and the data was extracted. Experimental results have shown to possess excellent NLO behavior, making them suitable for various optical applications in continuous wave domain.

## **2. Experimental Section**

### **2.1. Materials :**

Nickel (II) nitrate hexahydrate (Ni(NO<sub>3</sub>)<sub>2</sub>·6H<sub>2</sub>O) (99.9%), Sodium tungstate dehydrate (Na<sub>2</sub>WO<sub>4</sub>·2H<sub>2</sub>O) (99.9%), Europium (III) nitrate (Eu(NO<sub>3</sub>)<sub>3</sub>·6H<sub>2</sub>O) (99.9%) were purchased from Alfa Aaser. The above mentioned chemicals were used in the experiment as purchased without any further purification. Throughout the experiment double deionised water was used.

### **2.2. Synthesis of NiWO<sub>4</sub> nanostructures**

NiWO<sub>4</sub> nanostructures were synthesized by chemical precipitation technique. In this method 0.5 M of Ni(NO<sub>3</sub>)<sub>2</sub>·6H<sub>2</sub>O solution was slowly dropped into 0.5 M of Na<sub>2</sub>WO<sub>4</sub>·2H<sub>2</sub>O at 6ml/min of dropping rate under vigorous stirring. Slowly the color of the solution was turned into pale green, the indication of the formation of nickel tungstate nanoparticles. Then the solution was centrifuged at 10000 rpm for 10minutes for several times in order to ensure the complete removal of byproduct. At last the sample was washed with absolute ethanol and dried in hot air oven at 353K for 30 minutes. Then the sample was annealed in furnace at 873K for three hours with the heating rate of 2<sup>0</sup>C/min. For europium doping different concentration of Eu(NO<sub>3</sub>)<sub>3</sub>·6H<sub>2</sub>O (0.3, 0.5 and 0.7 wt% ) was added with respect to Ni<sup>2+</sup> ion concentration and same procedure was followed as mentioned above without any change. Finally, the annealed sample was grained into fine powder and preserved for further studies.

## **3. Result and discussion**

### **3.1. XRD pattern**

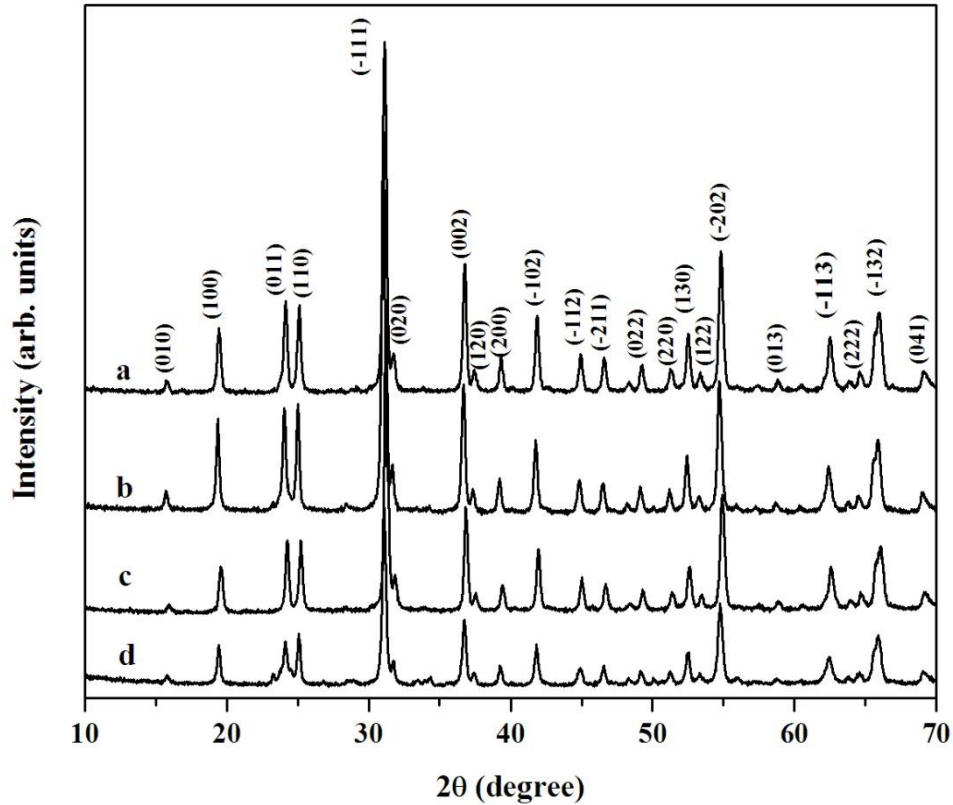


Fig.1 XRD patterns of (a) pure, (b) 0.3 (c) 0.5 & (d) 0.7  $\text{Eu}^{3+}$  doped  $\text{NiWO}_4$  nanostructures

The XRD pattern of pure and  $\text{Eu}^{3+}$  doped  $\text{NiWO}_4$  nanostructures are shown in fig.1. For pure  $\text{NiWO}_4$  nanostructures the diffraction peaks originated at (010), (100), (011), (110), (-111), (020), (002), (-102), (-202), (-113) and (-132) planes are indexed to monoclinic wolframite phase with space group  $P_{2/c}$  in accordance with JCPDS data card no: 00-015-0755 [19]. No impurity peaks can be seen which confirms the synthesized samples are pure and crystalline in nature. This shows that Eu doping does not induce any significant change in phase during synthesis and have entered the host lattice without affecting the crystal structure. It is observed that the addition of  $\text{Eu}^{3+}$  dopant ions decreases the intensity of the diffraction peaks of  $\text{NiWO}_4$  indicating the substitution of  $\text{Eu}^{3+}$  ( $1.06\text{\AA}$ ) causes lattice distortion into  $\text{Ni}^{2+}$  ( $0.7\text{\AA}$ ). As the doping concentration increases, the incorporation of Eu into the crystal lattice increases and causes lattice distortion due to its large size.

### 3.2. Field emission scanning electron microscope (FESEM)

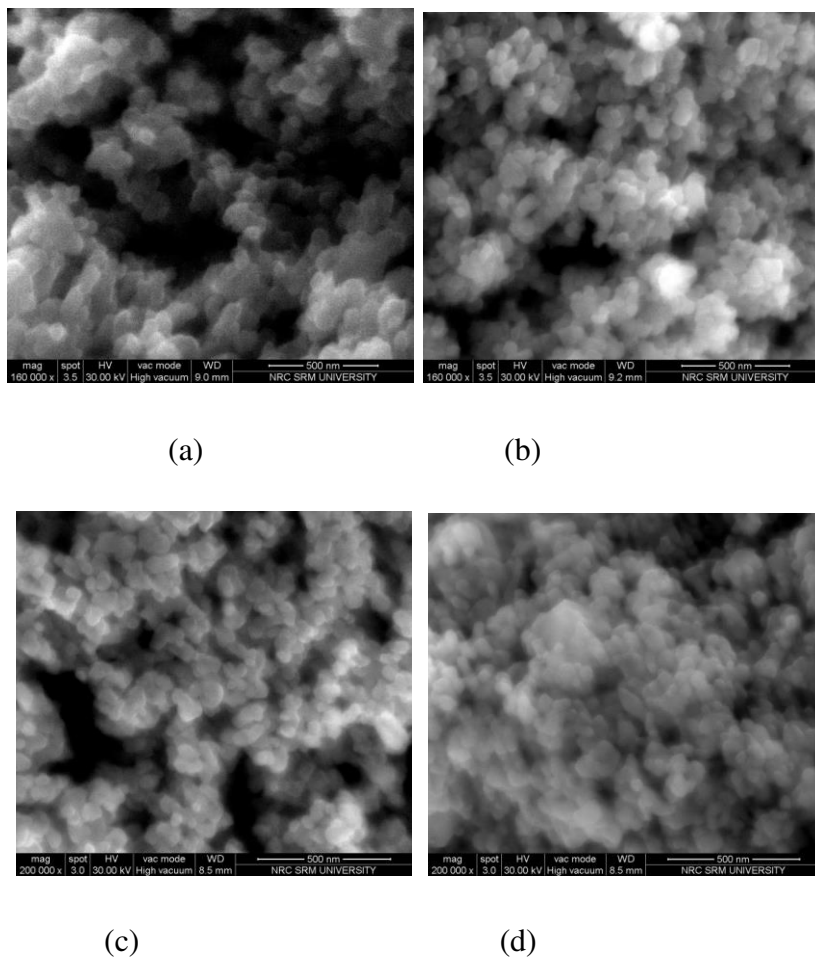


Fig.2. FESEM image of (a) pure, (b) 0.3 (c) 0.5 & (d) 0.7 Eu<sup>3+</sup> doped NiWO<sub>4</sub> nanostructures

The morphology of pure and Europium doped NiWO<sub>4</sub> nanostructures are shown in fig.2. The morphology of pure NiWO<sub>4</sub> nanostructures shows cubical shape with an average particle size between 40 and 50 nm. The particles are well dispersed and uniformly distribution of particle. It is quite interesting to note that the diameter of the particle decreases as doping concentration increases with similar morphology. This indicates doping of Eu does not influence the surface morphology rather restricts the growth of crystal at higher doping concentration.

### 3.3. Diffused reflectance UV spectroscopy

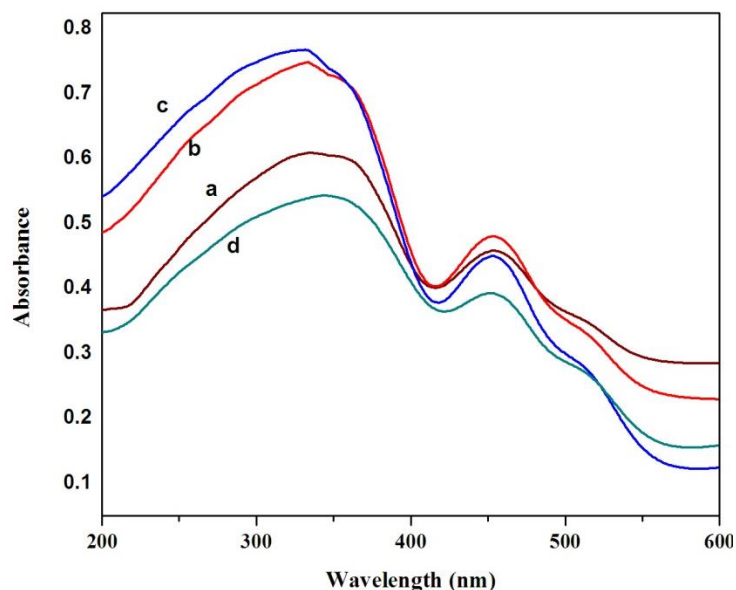


Fig.3. UV-vis spectra of (a) pure (b) 0.3 (c) 0.5 & (d) 0.7 %  $\text{Eu}^{3+}$  doped  $\text{NiWO}_4$  nanostructures

The optical absorption spectra of  $\text{NiWO}_4$  nanostructures are shown in fig.3. Both pure and  $\text{Eu}^{3+}$  doped  $\text{NiWO}_4$  nanostructures showed an excellent absorption in the UV region around 250 to 400nm with the shoulder peak occurred at 450nm. The absorption band appeared at 450nm is mainly due to transition of electron from  $^3\text{A}_{2g}$  to  $^1\text{E}_g$  [20]. The occurrence of absorption in the UV region is mainly due to excitation from  $\text{O}_{2p}$  to  $\text{Wt}_{2g}$  in the  $(\text{WO}_4^{2-})$  group and the peak appeared in the visible region is due to charge transfer of oxygen 2p atom to one of the empty 5d orbital of tungsten. The broad absorption occurred at the region from 250-400nm is due to small crystal size which in turn causes a strong quantum confinement effect on electron transition in nanocrystals [21].

### 3.4. Raman spectroscopy

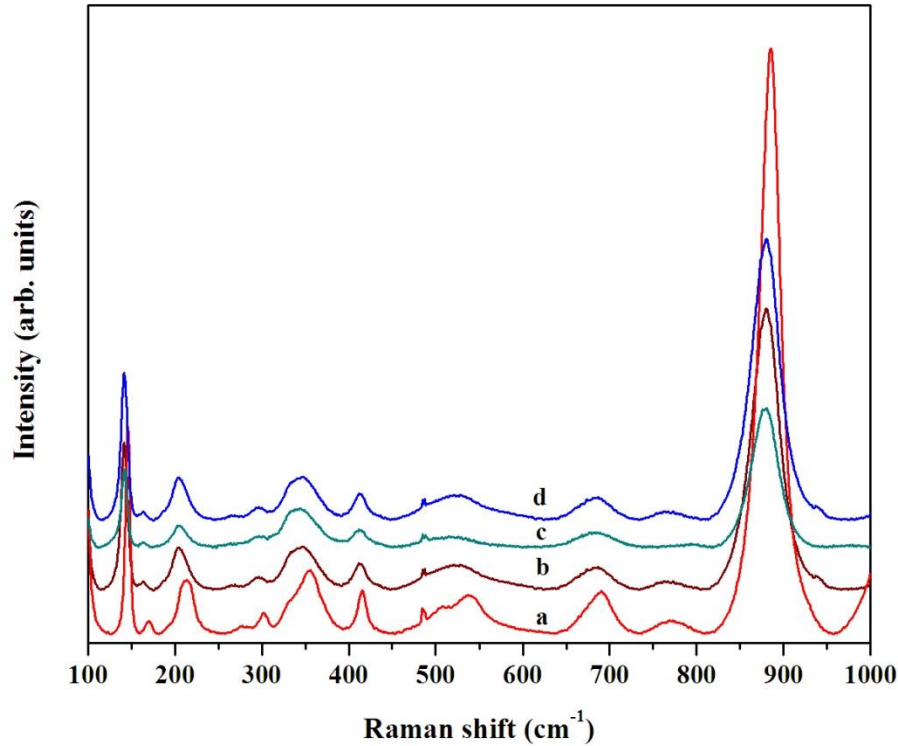


Fig.4. Raman spectra of (a) pure (b) 0.3 (c) 0.5 & (d) 0.7 %  $\text{Eu}^{3+}$  doped  $\text{NiWO}_4$  nanostructures

The Raman spectra of Eu doped  $\text{NiWO}_4$  nanostructures are shown in fig. 4. For monoclinic wolframite structure belonging to  $P_{2/c}$  space group, the Raman active vibration modes are grouped into six internal stretching modes caused by each of the six W-O bonds in the  $\text{WO}_6$  octahedrons. Group theory calculation of the monoclinic  $\text{NiWO}_4$  predicts 36 possible lattice modes represented as

$$\Gamma = 8A_g + 10B_g + 8A_u + 10B_u$$

The (g) vibrations are Raman active modes and (u) modes are infrared active. For pure and  $\text{Eu}^{3+}$  doped  $\text{NiWO}_4$  nanostructures show strong vibrations at 891, 778 and 698  $\text{cm}^{-1}$  and weak vibrations at 552, 340, 141, 203 and 170  $\text{cm}^{-1}$  are observed. It is reported that these peaks are attributed to normal W-O vibration of the  $\text{WO}_6$  octahedra [22]. The higher intensity modes at 891  $\text{cm}^{-1}$  corresponds to symmetric vibrations of short W-O bonds associated with the  $\text{WO}_6$  symmetric stretching vibration of highly covalent bonds. The modes at 778 and 698  $\text{cm}^{-1}$  are assigned to asymmetric vibrations of short W-O terminal bonds W-O-W bridges [23]. The modes observed in the frequency range between 500 -300  $\text{cm}^{-1}$  correspond to shorter and longer in-

plane W-O bonds whereas the active modes below  $350 \text{ cm}^{-1}$  are assigned to out-of-plane vibrations of W-O bonds and lattice vibrations in the wolframite structure [24]. As the Raman active modes are quite sensitive to the nature of bonding and cation distribution at respective sites, the doping of  $\text{Eu}^{3+}$  at  $\text{Ni}^{2+}$  sites have shown a decrease in the peak intensities and considerable shift of active modes at lower frequencies. The randomized distribution of Eu substitution in  $\text{NiWO}_4$  and changes in Eu-oxygen bond length might be responsible for these changes in the active modes.

### 3.5 Nonlinear optical studies

The third order NLO property of  $\text{Eu}^{3+}$  doped  $\text{NiWO}_4$  nanostructures with various concentrations of Eu have been studied by a Z-scan technique. To determine the nonlinear absorption and refraction coefficients of these nanostructures, both Open aperture (OA) and closed aperture (CA) Z-scan measurements were performed at 532 nm under cw laser excitation conditions. The results of the open aperture Z-scan shows a decrease in transmittance as the samples move towards the focal intensity (at  $Z=0$ ) indicating the presence of induced absorption in the samples and display an asymmetrical peak with respect to the focus as shown in the Fig. 5. This indicates the occurrence of reverse saturation absorption (RSA) process is dominant in these nanoparticles. RSA occurs when the absorption cross section of the excited state exceeds the ground state. It is clearly observed from the data that the transmittance at the focus decreases with increase in  $\text{Eu}^{3+}$  concentration and thus enhancing the valley. Different possible mechanisms such as two photon absorption (2PA), free carrier absorption and excited state absorption (ESA) are accountable for the observed nonlinear absorption (NLA) behavior. As the continuous laser is used in our experiment therefore the observed nonlinearity is due to thermal effects which increase ESA [25]. Thus the nonlinear mechanism leading to the observed nonlinearity is due to ESA assisted RSA in the nanostructures.

The absorption coefficient  $\beta$  of the nanoparticles under cw laser illumination are being estimated by the formalism.

$$T(Z) = 1 - \frac{\beta I_0 L_{eff}}{2\sqrt{2} \left(1 + \frac{Z^2}{Z_0^2}\right)}$$

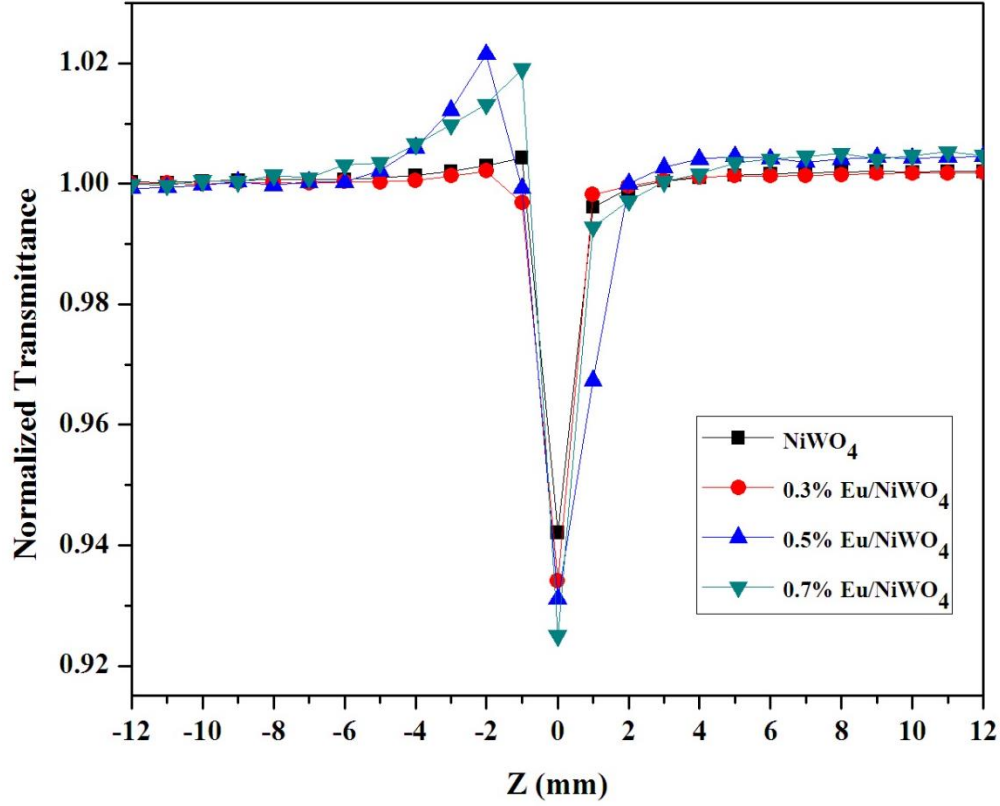


Fig.5. Open aperture Z-scan data of  $\text{Eu}^{3+}$  doped  $\text{NiWO}_4$  nanostructures

$I_0$  is the intensity of the laser beam at the focus ( $Z=0$ ),  $L_{\text{eff}}$  is the effective thickness of the sample

$$L_{\text{eff}} = \frac{[1 - \exp(-\alpha L)]}{\alpha}$$

$\alpha$  is the linear absorption coefficient at the laser excitation wavelength and  $L$  is the thickness of the sample. The nonlinear absorption coefficient ( $\beta$ ) is found to be  $10^{-6}$  (cm/W). The imaginary part of the third order nonlinear susceptibility can be determined from the nonlinear absorption coefficient by the following equation.

$$I_m \chi^{(3)}(\text{esu}) = 10^{-2} \frac{\varepsilon_0 c^2 n_0^2 \lambda}{4\pi^2} \beta (\text{cm/W})$$

Where  $c$  is the velocity of the light and  $n_0$  is the linear refractive index.

The closed aperture Z-scan data for the nanostructures are shown in fig.6. Both sign and magnitude of the nonlinear refractive index can be determined by this method. the recorded closed aperture curves show prefocal peak followed by post focal valley indicating that the

materials exhibit negative nonlinear refractive index. This signifies the self-defocusing nature of the materials. The physical origin of nonlinear refraction at cw laser regime can be electronic, molecular, electrostrictive or thermal in nature. As the cw laser produce weak electronic effect, the origin of nonlinearity cannot be explained by multiphoton absorption, therefore the originated nonlinearity is purely due to thermal effect. Due to thermal stress the thermal lens diverges and leads to variation of refractive index as a function of temperature which exhibits negative nonlinearity in the nanostructures. The material exhibiting thermal nonlinearity will focus (or) defocus the incident light. Therefore the existence of nonlinear refractive index is dominated by thermal effects.

The measurable quantity  $\Delta T_{p-v}$  can be obtained from the difference between the normalized peak valley and transmittance valley (TP-TV). The variation of this quantity in terms of the on-axis phase shift  $|\varphi_0|$  at the focus is given by [26]

$$\Delta T_{p-v} = 0.406(1 - S)^{0.25}|\varphi_0|$$

Where  $\Delta\varphi_0$  is the on-axis phase shift at the focus,  $S$  is the aperture linear transmittance and is given by  $S = 1 - \exp(-2r_a^2/\omega_a^2)$  is the linear aperture transmittance.  $r_a$  denotes the aperture radius and  $\omega_a$  denotes the radius of the laser spot before the aperture.

Then nonlinear refractive index is given by

$$n_2 = \frac{\Delta\varphi_0\lambda}{2\pi I_0 L_{eff}} \left( \frac{cm^2}{W} \right)$$

Where  $\lambda$  is the laser wavelength,  $I_0=1.1kW/cm^2$  is the input intensity and  $L_{eff}$  is the effective length of the sample.

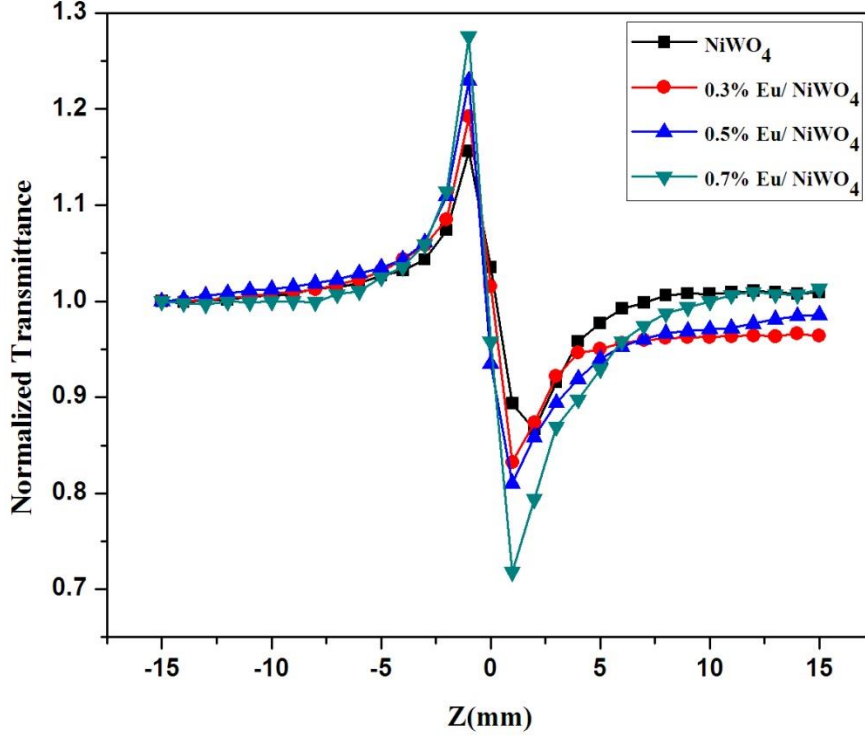


Fig. 6. Closed aperture Z-scan data of  $\text{Eu}^{3+}$  doped  $\text{NiWO}_4$  nanostructures

The real part of the third-order nonlinear susceptibility  $\chi^{(3)}$  were deduced from the following equation

$$\text{Re}\chi^{(3)}(\text{esu}) = 10^{-4} \frac{\epsilon_0 c^2 n_0^2}{\pi} n_2 (\text{cm}^2/\text{W})$$

where  $\epsilon_0$  is permittivity of the vacuum,  $n_0$  is the linear refractive index of the sample, and  $C$  is the velocity of light in vacuum. Finally, the absolute value of the third order susceptibility  $\chi^{(3)}$  can be obtained given by following equation [27]:

$$|\chi^{(3)}| = [(\text{Re}\chi^{(3)})^2 + (\text{Im}\chi^{(3)})^2]^{1/2}$$

The acquired z-scan data clearly indicates that  $\text{Eu}^{3+}$  doped nanostructures exhibits good third order NLO properties compared to pure  $\text{NiWO}_4$  which is enumerated in Table 1. The nonlinear values computed are in good agreement with the previous reported results. Tamgadge et al.

reported NLO studies on Sr-CuO PVA nanocomposite thin films [28], where  $\beta$  was calculated in the order of  $10^{-6}$  cm/W. The substitution of Eu at the lattice sites of Ni has greater influence of widening the band gaps. After the substitution of  $\text{Eu}^{3+}$ , the NLO appears a step rise, indicating that the possibility of enhancing the NLO effect by tuning the band gap. The high magnitude of the observed nonlinearity can be primarily due to thermal change in the sample.

Table.1 Comparison of nonlinear optical parameters of  $\text{Eu}^{3+}$  doped  $\text{NiWO}_4$  nanoparticles

<b>Samples parameters</b>	<b><math>\text{NiWO}_4</math></b>	<b>0.3 %Eu</b>	<b>0.5 %Eu</b>	<b>0.7 %Eu</b>
<b>Nonlinear refractive index, <math>n_2 \times 10^{-10}</math> cm<sup>2</sup>/W</b>	3.38	2.42	2.97	4.42
<b>Nonlinear absorption coefficient, <math>\beta \times 10^{-6}</math> cm/W</b>	6.2	7.46	7.04	8.16
<b>Real part of third order nonlinear refractive index <math>\text{Re } \chi^{(3)} \times 10^{-8}</math> esu</b>	4.04	2.81	3.45	5.19
<b>Imaginary part of third order nonlinear refractive index, <math>\text{Im } \chi^{(3)} \times 10^{-7}</math> esu</b>	3.14	3.67	3.47	4.06
<b>Third order nonlinear optical susceptibility, <math>\chi^{(3)} \times 10^{-7}</math> esu</b>	3.16	3.68	3.48	4.09

#### 4. Conclusions

$\text{Eu}^{3+}$  doped  $\text{NiWO}_4$  nanostructures with various concentration of  $\text{Eu}^{3+}$  were prepared by a chemical precipitation technique. The structural, optical and morphological characterization as a function of doping concentration was studied. XRD results revealed that the nanostructures exhibit monoclinic wolframite structure with space group  $P_{2/c}$ . The variation of peak width and intensity of Raman active modes confirms the incorporation of Eu in  $\text{NiWO}_4$ . Third order nonlinear studies were done by a Z-scan technique at 532 nm using a continuous wave Nd:YAG laser. Open aperture and close aperture traces have shown that the occurrence of the observed nonlinearity is mainly due to reverse saturable absorption and negative nonlinear refractive index. The results suggest the possibility that the incorporation of Eu into  $\text{NiWO}_4$  have potential to be used photonic device applications.

#### References

- [1] K.Vasudevan, M.C.Divyasree, K.Chandrasekharan, Optics & Laser Technology, Volume 114 (2019) 35-39
- [2] G. Jagannath, B. Eraiah, K. Naga Krishnakanth, S.Venugopal Rao, Journal of Non-Crystalline Solids Volume 482, ( 2018) 160-169
- [3] U. Nithiyantham, Sivasankara Rao Ede, S. Anantharaj, and Subrata Kundu, *Cryst. Growth Des.* 2015, 15, 2, 673-686
- [4] H. Wang, F.D. Medina, Y.D. Zhou, Q.N. Zhang, Temperature dependence of the polarized Raman spectra of ZnWO<sub>4</sub> single crystals, *Phys. Rev. B* 45 (1992) 10356–10362.
- [5] .C. Pullar, S. Farrah, N.McN. Alford, *J. Eur. Ceram. Soc.* 27 (2007) 1059–1063
- [6] T. Montini, V. Gombac, A. Hameed, L. Felisari, G. Adami, P. Fornasiero, Synthesis, characterization and photocatalytic performance of transition metal tungstates, *Chem. Phys. Lett.* 498 (2010) 113–119.
- [7] Seied Mahdi Pourmortazavia, Mehdi Rahimi-Nasrabadi, Morteza Khalilian-Shalamzarib, Mir Mahdi Zahedic, Seiedeh Somayyeh Hajimirsadeghic, Ismail Omranib; Synthesis, structure characterization and catalytic activity of nickel tungstate nanoparticles; *Applied Surface Science* 263 (2012) 745–752.
- [8] H M. Maczka, P.T.C. Freire, A. Majchrowski, P.S. Pizani, I.V. Kityk, *J. Alloys Compd* 579 (2013) 236-242  
Mehdi Rahimi-Nasrabadi, Seied Mahdi Pourmortazavi, Mohammad Reza Ganjali, Ali Reza Banan, Farhad Ahmadi, *Journal of Molecular Structure*, Volume 1074, 25 (2014), Pages 85-91
- [9] J. Zhang, Z. Zhang, W. Zhang, Q. Zheng, Y. Sun, C. Zhang, X. Tao, *Chem. Mater.* 23 (2011) 3752-3761.
- [10] V.I. Lukanin, D.S. Chunaev, A. Ya Karasik, *J. Exp. Theor. Phys.* 113 (2011) 412-421.
- [11] Shi, J. Meng, Y. Ren, Q. Su, Structure, Luminescence and magnetic properties of aglnwzog (Ln =Eu, Gd, Tb and Dy) compounds, *J.phys. Chem Solids* 59 (1998) 105-110.
- [12] H. Wang, C.K. Lin, X.M. Liu, J. Lin, and M. Yu, *Appl. Phys.Lett.* 87 (2005)181907.
- [13] A Guang Jia, Dongbing Dong, Changying Song, Lanfen Li, Cuimiao Huang, Cuimiao Zhang, *Materials Letters* 120 (2014) 251–254
- [14] J.M. Quintana-Melgoza, J. Cruz-Reyes, M. Avalos-Borja, Synthesis and characterization of NiWO<sub>4</sub> crystals, *Mater. Lett.* 47 (2001) 314–318.
- [15] L. Zhang, C. Lu, Y. Wang, Y. Cheng, *Mater. Chem. Phys.* 103 (2007) 433–436.
- [16] J.H. Ryu, J.-W. Yoon, C.S. Lim, K.B. Shim, Microwave-assisted synthesis of MWO<sub>4</sub> and MMoO<sub>4</sub> (M= Ca, Ni) nano-powders using citrate complex precursor, *Key Eng. Mater.* 317–318 (2006) 223–226

- [17] J.H. Ryu, J.-W. Yoon, C.S. Lim, W.-C. Oh, K.B. Shim, *Ceram. Int.* 31 (2005) 883–888.
- [18] Xuansheng Feng, Ying Huang\*, Menghua Chen, Xuefang Chen, Chao Li, Suhua Zhou, Xiaogang Gao, *Journal of Alloys and Compounds* 763 (2018) 801-807
- [19] Seied Mahdi Pourmortazavia, Mehdi Rahimi-Nasrabadi, Morteza Khalilian-Shalamzari, Mir Mahdi Zahedi, Seiedeh Somayyeh Hajimirsadeghi, Ismail Omrani, *Applied Surface Science* 263 (2012) 745–752
- [20] A Siti Murni M Zawawi, Rosiyah Yahya, Aziz Hassan, H N M Ekramul Mahmud and Mohammad Noh Daud, Structural and optical characterization of metal tungstates ( $MWO_4$ ;  $M=Ni, Ba, Bi$ ) synthesized by a sucrose-templated method. *Chemistry Central Journal* 7 (2013) 8
- [21] Z. Song, J. Ma, H. Sun, W. Wang, Y. Sun, L. Sun, Z. Liu, C. Gao, Synthesis of  $NiWO_4$  nano-particles in low-temperature molten salt medium, *Ceram. Int.* 35 (2009) 2675–2678.
- [22] Siti Murni M Zawawi, Rosiyah Yahya, Aziz Hassan, H N M Ekramul Mahmud and Mohammad Noh Daud, *Chemistry Central Journal* 7 (2013) 80
- [23] S. D. Ramarao and V. R. K. Murthy, *Dalton Trans.*, 2015,44, 2311-2324
- [24] M. Daturi, G. Busca, M. M. Borel, A. Leclaire and P. Piaggio, *J. Phys. Chem. B*, 101 (1997) 4358.
- [25] A F.Z. Henari, Optical switching in organometallic phthalocyanine, *J. Opt. A: Pure Appl. Opt.* 3 (2001) 188–190.
- [26] S. Yuvaraj, N. Manikandan, G. Vinitha, *Optical Materials* 73 (2017) 428-436
- [27] Imad Al-Deen Hussein Al-Saidi, Saif Al-DeenAbdulkareem, Nonlinear optical properties and optical power limiting behavior of Leishman dye in solution and solid polymer film using Z-scan, *Optik* 126 (2015) 4299–4303.
- [28] Y.S. Tamgadge, S.S. Talwatkar, A.L. Sunatkari, V.G. Paturkar, G.G. Muley, *Thin Solid Films* 595 (2015) 48-55.